J. Cent. South Univ. (2021) 28: 1966−1977
DOI: https://doi.org/10.1007/s11771-021-4745-3

Springer

Sintering microstructure and properties of copper powder prepared by electrolyzation and atomization

LI Pei(李沛)[1], CHEN Cun-guang(陈存广)[1, 2, 3], QIN Qian(秦乾)[1], LU Tian-xing(陆天行)[1], SHAO Yan-ru(邵艳茹)[1], YANG Fang(杨芳)[1, 3], HAO Jun-jie(郝俊杰)[1], GUO Zhi-meng(郭志猛)[1, 3]

1. Institute for Advanced Materials and Technology, University of Science and Technology Beijing, Beijing 100083, China;
2. State Key Laboratory for Advanced Metals and Materials, University of Science and Technology Beijing, Beijing 100083, China;
3. Innovation Group of Marine Engineering Materials and Corrosion Control, Southern Marine Science and Engineering Guangdong Laboratory (Zhuhai), Zhuhai 519000, China

Abstract: The almost completely dense copper was prepared by ultrafine copper powder prepared with both methods of electrolysis and novel water-gas atomization through cold isostatic pressing (CIP) and sintering under atmospheric hydrogen. Fine copper powder possesses the higher sintering driving force, thereby promoting shrinkage and densification during the sintering process. The grain size of sintered samples by electrolytic copper powder is smaller than that prepared by the atomized copper powder, and the twin crystals are particularly prone to forming in the former sintered microstructure due to the raw powder with low oxygen content and high residual stress originating from the CIP process. The relative density of samples by electrolytic and atomized powder at 1000 °C sintering temperature achieves 99.3% and 97.4%, respectively, significantly higher than that of the powder metallurgy copper parts reported in the literature. Correspondingly, the ultimate tensile strength and yield strength of samples by both kinds of copper powder are approximately similar, while the elongation of the sintered sample by the electrolytic powder (60%) is apparently higher than the atomized powder (44%). The superior performance of samples fabricated by electrolytic powder is inferred from the full density and low oxygen level for there is no cuprous oxide in the grain boundaries.

Key words: copper powder; electrolyzation; gas-water combined atomization; sintered microstructure; property

Cite this article as: LI Pei, CHEN Cun-guang, QIN Qian, LU Tian-xing, SHAO Yan-ru, YANG Fang, HAO Jun-jie, GUO Zhi-meng. Sintering microstructure and properties of copper powder prepared by electrolyzation and atomization [J]. Journal of Central South University, 2021, 28(7): 1966−1977. DOI: https://doi.org/10.1007/s11771-021-4745-3.

1 Introduction

Ranking second in the consumption of non-ferrous metals, copper is widely used in electrical, mechanical manufacturing, and construction industries, due to excellent electrical and thermal conductivity, corrosion resistance, and adequate strength [1, 2]. Due to the advantages of the fine and uniform microstructure, the flexibility of composition control, near-net forming and relatively low temperature sintering, powder manufacturing (PM) has become an attractive technology to develop novel copper and copper alloys. It is worth noting

Foundation item: Project(92066205) supported by the National Natural Science Foundation of China; Project(2019-Z10) supported by the State Key Lab for Advanced Metals and Materials of China; Project(FRF-MP-20-52) supported by the Fundamental Research Funds for the Central Universities, China
Received date: 2020-12-28; **Accepted date:** 2021-04-07
Corresponding author: CHEN Cun-guang, PhD, Research Assistant; Tel: +86-10-62334341; E-mail: cgchen@ustb.edu.cn; ORCID: https://orcid.org/0000-0002-6525-228X

that the physical and mechanical properties of copper and copper alloy structural parts manufactured by PM have been comparable to traditional casting and forging. Such superior properties are depended on high quality powder and high sintered density in the PM process [3].

It is believed that excellent mechanical properties can be obtained by increasing sintering activity, which can be realized by using ultrafine and hypoxic powder especially for copper. Copper powder has been produced with various approaches such as chemical precipitation, electrolytic deposition, oxidation and reduction, water atomization, gas atomization, water-gas combined atomization [4−8]. Among these methods, the electrolytic deposition and water-gas combined atomization are known as the appropriate process for preparing fine powder. The undesirable effect is easy absorption of oxygen from the air on account of high surface energy of fine powder. The oxidation leads to the degradation of powder quality [9−11]. Even though the degree of oxidation is low, a layer of oxide film is apt to covering the powder surface [12, 13]. Since metal powder is extremely sensitive to oxygen and usually coated with natural oxide films, the sintering is often carried out under reducing atmosphere or vacuum [14−16].

For copper sintering, the compact tends to cause expansion because of the formation of water vapor during sintering in hydrogen atmosphere. Thus, controlling the oxygen content is a key problem encountered in copper sintering [17−20]. It is regarded that reducing the oxygen content can significantly drop off the swelling effect [21, 22]. Besides, the researchers took other steps to achieve densification of copper powder, including powder pressing, sintering and re-pressing, which can acquire the required electrical conductivity and mechanical properties [23]. Currently, many rapid densification processes have gradually been developed, such as spark plasma sintering (SPS), microwave sintering (MS), and hot-pressed sintering (HP) [24, 25]. The above rapid densification processes can consolidate the copper powder at a relatively fast rate and obtain a bulk material with high density. However, the related equipment is extremely expensive, and it is difficult to meet the requirements of industrial production [17]. The reports about high-density PM Cu produced by atmospheric sintering are rare.

Furthermore, fine powder particles possess more powder particle interfaces so as to easily exhaust the water vapor, weakening the effect of sintering expansion. Also, fine powder can provide higher driving force during sintering [26], and is conducive to develop into uniform microstructure with fine grains. Based on this, oil-bearings, friction materials and electrical parts can be made of copper and copper alloy fabricated by PM [27−29]. In this study, the sintering behavior with varying sintering temperature in hydrogen atmosphere was investigated for two kinds of coper powder with approximately the same average particle size (~10 μm), prepared by the electrolytic deposition and water-gas combined atomization. The density, microstructure and mechanical properties of the samples were studied in detail, and the related mechanism of sintered densification and performance changes was also analyzed.

2 Experimental

The starting materials in this study are electrolytic copper powder made by GRIPM Advanced Materials Co., Ltd., and water-gas atomized copper powder made by Yahao Material & Technology Co., Ltd. Two kinds of powders were first compacted by cold isostatic pressing (CIP). Then, hydrogen atmosphere sintering was constructed with the constant heating rate of 10 °C/min according to the sintering curve as shown in Figure 1. It is necessary to keep the temperature at 400 °C for 2 h to remove the gas adsorbed on the powder surface and reduce some oxides. The sintering temperature was 700, 800, 900 and 1000 °C for 2 h. The hydrogen flow rate was 2 L/min.

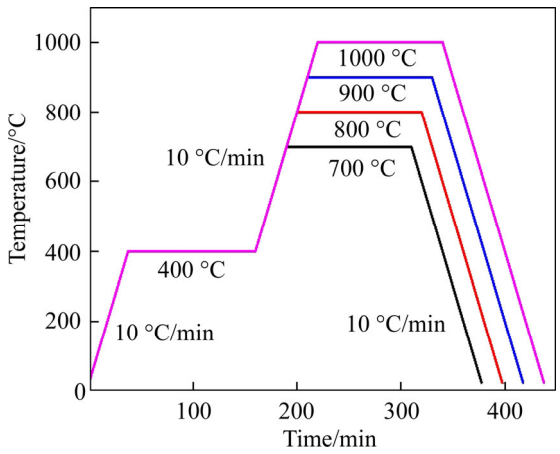

Figure 1 Schematic diagram of fabricating process

The particle size of two kinds of copper powders was determined using a laser diffraction system (BT-9300S) by wet dispersion. An optical microscopy (OLYMPUS CX41-12C02) and a field emission scanning electron microscope (FESEM, ZEISS SUPRA^{TM} 55) were used to examine the morphology of powders, and the microstructure and fracture surface morphology of sintered samples. The Archimedes method was applied to measure the density for each sample (ASTM B962-13) [30]. The oxygen content of samples was measured by non-dispersive infrared gas analysis with the ELTRA ONH-2000 apparatus. The relative density was calculated in terms of the theoretical density of copper, 8.96 g/cm^3 [31]. The uniaxial tensile tests of sintered samples were carried out on a MTS810 testing machine according to the ASTM-E08 standard. All the tensile specimens with the gage diameter of 5 mm and the gage length of 25 mm were tested with a constant speed of 0.5 mm/min at room temperature.

3 Results and discussion

3.1 Powder morphology and particle size distribution

Figure 2 displays the powder morphology with the particle size distribution. In this study, atomized copper powder and electrolytic copper powder were used as raw materials. As shown in Figures 2(a) and (b), large particles in electrolytic copper powder are composed of multiple nearly spherical primary particles, exhibiting concentrated granularity distribution. The particle size distribution of electrolytic copper powder is D_{10}=5.8 μm, D_{50}=12.0 μm and D_{90}=25.0 μm. Using Nano Measurer software, an average primary particle size is calculated to be 2.22 μm. The water-gas combined atomized copper powder with spherical morphology is clearly seen in Figure 2(c), and the particle size distribution is D_{10}=3.3 μm, D_{50}=10.2 μm and D_{90}=28.0 μm, as presented in Figure 2(d). During the water-gas combined atomization, the melt liquid of copper is broken up in two steps, i.e., first by a high-pressure gas jet and then by a low-pressure water jet, and further cooled by the water jet. It is a novel powder preparation technique unlike water atomization and gas atomization. The atomization system is optimized so that after the metal liquid is broken up by the nitrogen jet, when spheroidization of the droplets has completed but the droplets have not yet solidified, most droplets are cooled by water, and only a small number of large droplets are further broken up by the water. Therefore, the proportion of spherical powder in the water-gas combined atomized powder is relatively high.

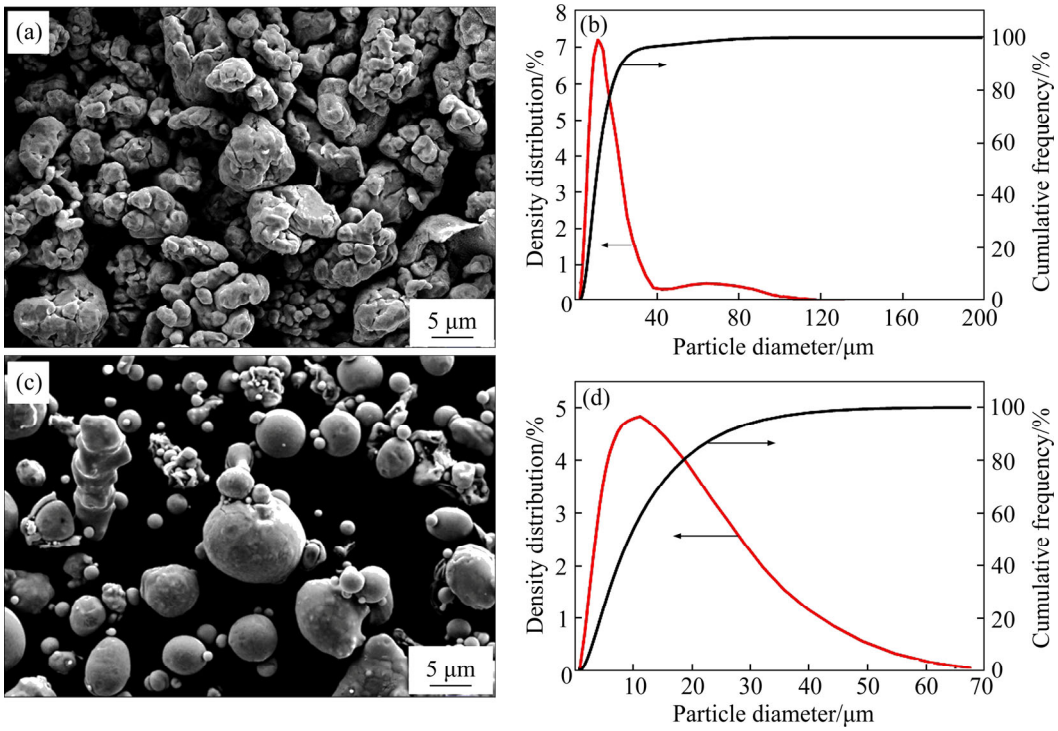

Figure 2 SEM images of powder and particle size distribution: (a, b) Electrolytic copper powder; (c, d) Atomized copper powder

3.2 Microstructure of sintered samples

The evolution of microstructure and pores of sintered samples at various sintering temperature was observed by optical micrographs (OM), as seen in Figures 3 and 4. It is similar for both sintered samples prepared by electrolytic and atomized copper powder that as raising the sintering temperature, the size of sintered neck increases, the grains become clearer and larger, and the pores gradually disappear and get rounded. Red arrows denote the large and irregular pores, and the yellow arrows indicate the small and round pores. In the case of electrolytic copper samples sintered at 700 °C, the pores are large and varied in shape. As the sintering temperature increases, the pores become more rounded. For samples sintered at 1000 °C, the pores become smaller and isolate from the pore network. Most of them are small spherical pores and a few large-sized irregular-shaped holes can be found.

However, the shape of pores in the sintered microstructure by atomized copper powder is slightly different from the ones consolidated by the

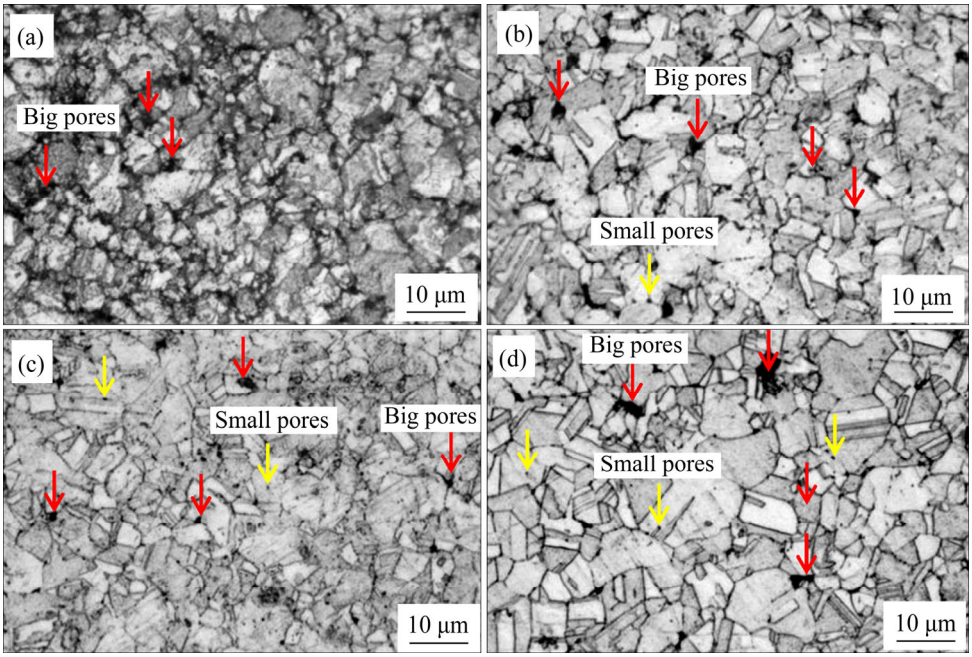

Figure 3 OM images of electrolytic copper powders sintered at: (a) 700 °C; (b) 800 °C; (c) 900 °C; (d) 1000 °C

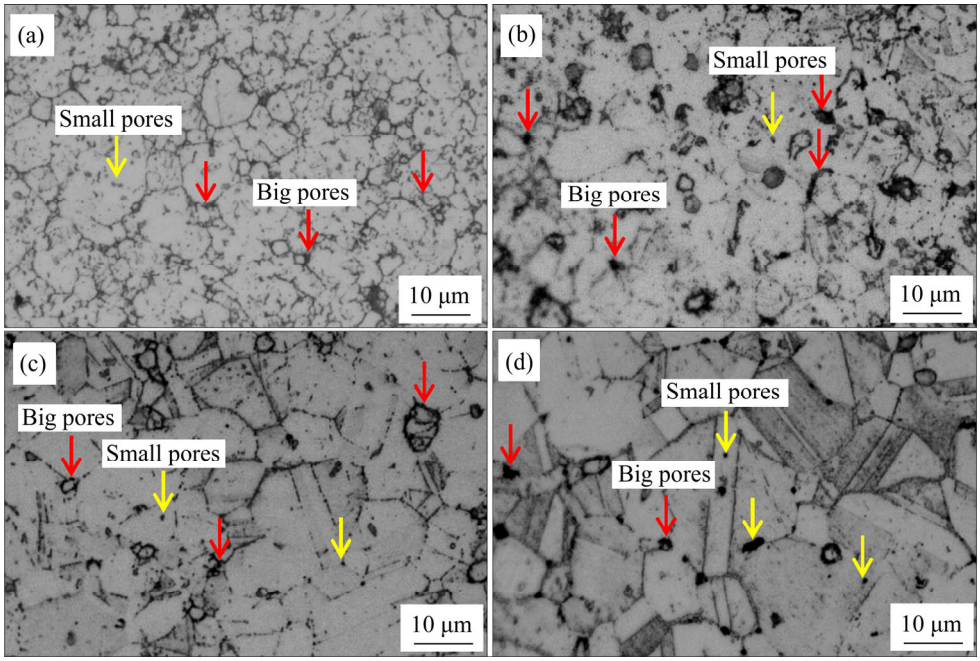

Figure 4 OM images of atomization copper powders sintered at: (a) 700 °C; (b) 800 °C; (c) 900 °C; (d) 1000 °C

electrolytic copper powder. First of all, due to the unclean surface of atomized copper, the absence of powder boundary is obvious. In atomized copper powder particles, most of the oxygen exists on the surface of the particles and the grain boundaries inside the particles in the form of cuprous oxide [32]. Therefore, there are obvious powder boundaries and spherical holes formed by hydrogen reduction of cuprous oxide in the grain boundaries in the early stage of sintering.

Variations in grain size and twin crystals are another important feature in both sintered samples. At the same sintering temperature, the grains of bulk samples by electrolytic copper powder are smaller than atomized copper powder on the whole. As for samples composed of electrolytic copper powder, there is no obvious annealing twins formed in the microstructure sintered at 700 °C as seen in Figure 3(a). When the sintering temperature rises up to 800 °C, a small number of incomplete twin crystals appear in Figure 3(b), which indicates that the twin crystals may not be fully developed during the sintering process. Increasing the sintering temperature to 900 °C, transgranular twin crystals come out besides the incomplete twins in Figure 3(c). Ultimately as shown in Figure 3(d), a large number of transgranular twins are generated at 1000 °C, and twin belts even form inside some grains. Nevertheless, there are still a small number of incomplete twins. It is clear that the appearance of twin crystals increases the number of grain boundaries, which can hinder the grain growth.

With regard to samples made from atomized copper powder, only a handful of twin crystals can be found when the samples are sintered at elevated temperature, such as 900 °C and 1000 °C, as seen in Figures 4(c) and (d). At lower sintering temperature (700 °C and 800 °C), twin crystals are barely visible in Figures 4(a) and (b). It is a very clear distinction about the formation temperature, size and distribution of twins between samples prepared by electrolytic copper powder and atomized copper powder. In addition, the grain size of sintered samples prepared by atomized copper powder is larger than that of electrolytic copper powder, as presented in Figures 3 and 4.

On the one hand, it is noted that the primary size of powder particles prepared by two mentioned techniques is different, seen from Figures 2(a) and (c). The primary size of electrolytic copper powder particles is 1−2 μm, whereas the size of copper powder particles fabricated by water-gas combined atomization is 2−10 μm. It is thus predicted that the deformation of powder particles is also different during the CIP process. Previous investigations have highlighted that there is a particle size dependence of the deformation, utilizing EBSD to analyze green compacts [33]. Specifically, smaller particles or small sections of larger particles have a larger fraction of their total volume deformed than large particles. The recovery and recrystallization will occur at elevated temperature during the subsequent sintering at the deformed regions with an increased amount of low-angle grain boundaries, indicating an increased dislocation density. Accordingly, for electrolytic copper powder particles, the larger strain energy inside the particles from the larger deformation in the CIP process can provide greater driving force for grain growth. This easily leads to the formation of annealing twins for copper with the face-centered cubic crystal structure at the high temperature sintering process.

On the other hand, for copper powder by water-gas combined atomization, the oxygen content is generally higher than electrolytic copper powder, although the average granularity is very close. This means that the atomized powder has higher sintering activity because of purification of powder particle surface by hydrogen reduction. Moreover, as the atoms can easily diffuse in the fine-grained recrystallized inter-particle regions, the magnitude of mass transfer and thus sintering are enhanced, resulting in apparent grain growth instead of the predominant formation of twin crystals.

3.3 Relative density

As is well known, the relative density of materials prepared by PM has a direct influence on their physical properties. The higher the relative density reaches, the closer the physical properties get to the theoretical values. Figure 5 shows that the influence of the sintering temperature on the relative density of samples by two kinds of powders. It can be seen that the higher the sintering temperature was, the higher the sintered density of two kinds of copper samples attained. The density of green compacts of electrolytic copper powder and atomized powder was 7.43 and 7.55 g/cm^3, respectively. The density variation was attributed to the good filling performance of spherical atomized powder.

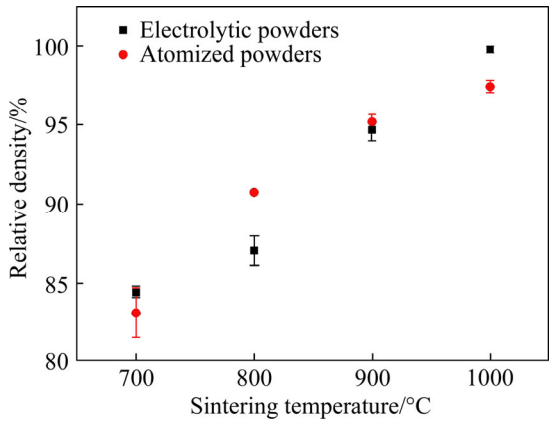

Figure 5 Influence of sintering temperature on relative density

When sintering at 700 °C, the relative density of samples by electrolytic copper powder is higher than that of copper powder by water-gas combined atomization, due to the higher sintering activity from the finer primary particles of electrolytic copper powder. However, the relative density of samples by atomized powder surpasses that by electrolytic powder as the sintering temperature is raised to 800 °C. The lower density of samples by electrolytic copper powder is clearly associated to the reduction of oxide inclusions and H_2O expansion inside the Cu particles, which lead to large pores as shown on the cross section of the sample (Figure 3(b)), while cross sections of samples by atomized powder only show intergranular pores and internal oxide inclusions (Figure 4(b)). As the sintering temperature increases further, a large number of obturator pores in the sintered body gradually shrink, and the number of pores decreases. The relative density of both kinds of samples is close to 95% after sintered at 900 °C. Furthermore, at the sintering temperature of 1000 °C, the relative density of samples by electrolytic and atomized copper powder reaches a maximum value, 99.3% and 97.4%, respectively. Despite some big pores can be discovered in the microstructure of copper sample by electrolytic powder, the micropores are almost completely gone. However, there are some pores hard to eliminate inside the grains and along the grain boundaries of copper sample by atomized powder, resulting in the limited density enhancement.

Using the fine powder for sintering, a particularly high density can be obtained. The main factors affecting copper powder sintering are particle size, temperature and pressure [34]. In pressureless sintering, the driving force for sintering comes from the excess surface energy of the system. In order to investigate the sintering mechanism of the high density of electrolytic copper, the sintering driving force of two kinds of copper powder was calculated by the following equation [35, 36]:

$$\Delta E=\gamma_{sv}W_mS_p\propto S_p \quad (1)$$

where ΔE is intrinsic excess surface energy driving force, γ_{sv} is the solid/gas interface energy, W_m is the molar mass of crystal material and S_p is the specific surface area of powder. Since the comparisons are all sintered copper materials, the solid/gas interface energy and molar mass are constant. It can be seen from formula (1) that ΔE is proportional to S_p. Therefore, the higher the specific surface area of powder, the higher the intrinsic excess surface energy driving force for sintering material.

In absence of an external driving force for sintering, the higher intrinsic excess surface energy driving force for sintering means the higher sintered density of the material, which is an important performance parameter of PM copper alloys. In this research, the specific surface area of electrolytic copper powder and atomization copper powder was calculated. Because the electrolytic copper powder is a secondary particle that consist of aggregated smaller primary particles, the value of average particle size is 2.22 μm. The average particle size of atomization powder is 10.2 μm. The S_p of electrolytic powder is 303.7 m^2/kg, which is five times that of atomization powder of 66.1 m^2/kg.

In addition, the oxygen content plays a very important role in the copper sintering process. Most oxygen on the powder surface exists in the form of CuO, Cu_2O and $Cu(OH)_2$, but the oxygen can be mostly removed when the powder or green body is reduced or sintered under a reducing atmosphere [37]. Usually, there is a polycrystalline microstructure with 1−2 μm grains prepared by atomization copper powder. Cu_2O precipitates of 0.5−1 μm are located at the grain boundaries or inside the grains. During the hydrogen reduction, hydrogen readily diffuses through solid copper to react with oxygen and form steam. The large steam molecules are unable to diffuse inside solid copper grains, but escape outward through grain boundaries, which was observed in the formation of blisters or cracks [38]. As shown in Figure 6(a), the widening of grain boundaries of atomized copper powder

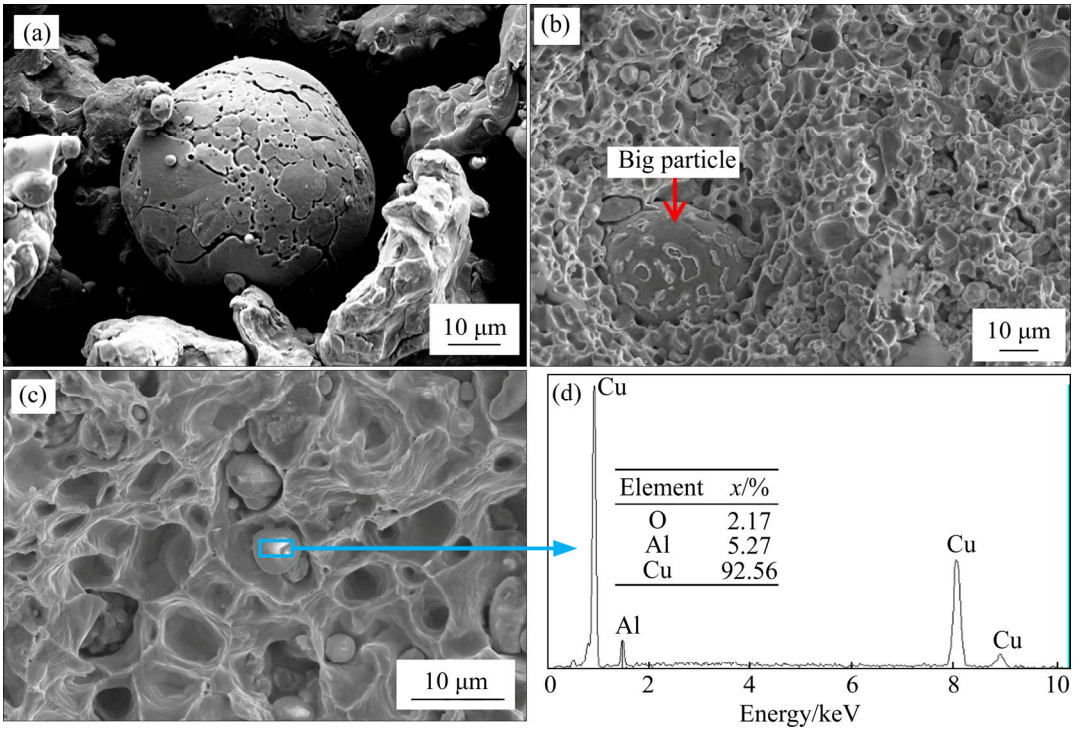

Figure 6 Surface of atomization powder particle after heat treatment (30 min) at 800 °C under H_2 (a), fracture surfaces of samples sintered at 800 °C (b, c), and EDS of spot in (c) with atomized copper powder (d)

particles reduced under hydrogen at 800 °C can be clearly found. Electrolytic copper powder has secondary particles consisted of aggregated smaller primary particles and every primary particle is a single grain. In that case, the steam phenomenon that could happen to atomization powder will not occur on electrolytic copper powder, so that the reduction reaction will proceed more thoroughly [39−41]. As a result, the samples prepared by electrolytic copper powder possess lower oxygen content and higher density.

The relationship between the sintering temperature and the oxygen content of electrolytic copper samples were investigated. Figure 7 shows that the oxygen content decreases with increasing sintering temperature. The oxygen content of original electrolytic copper powder is 0.2371 wt%, and sharply decreases when the sintering temperature is above 800 °C. Eventually, it reaches the minimum value of 0.0129 wt% after sintering at 1000 °C. Copper oxide is reduced by hydrogen during sintering. Owing to the low compacting pressure, the degassing can be thoroughly carried out, which is beneficial for improving the density.

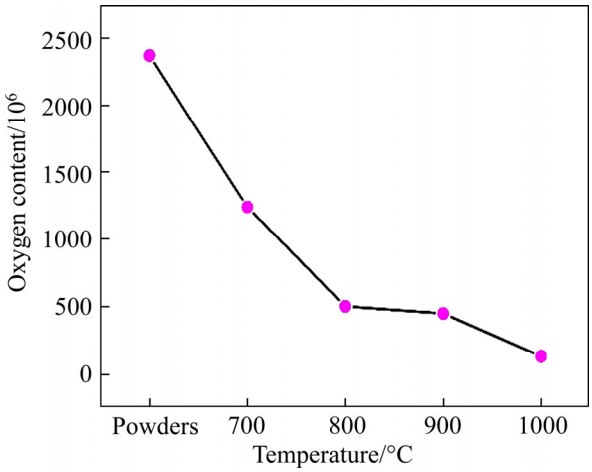

Figure 7 Oxygen content of samples sintered at: (a) 700 °C; (b) 800 °C; (c) 900 °C; (d) 1000 °C with electrolytic copper powder

3.4 Mechanical properties

Under the same condition of the preparation process, the samples by electrolytic copper powder have higher density than atomized copper powder at higher temperature. The mechanical properties of two kinds of sintered copper samples were analysed. Figures 8 and 9 show that the mechanical properties are reinforced with the increasing sintering temperature.

In general, pores in PM products adversely affect the mechanical properties. The ultimate tensile strength (UTS), yield strength (YS) and elongation

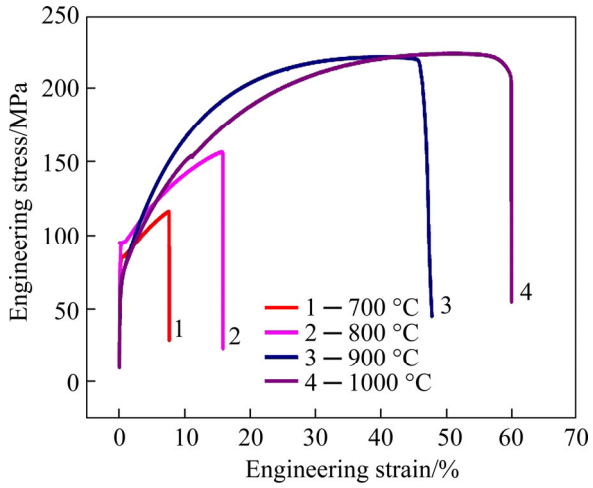

Figure 8 Room temperature engineering strain vs stress curves for sintered samples with electrolytic copper powder

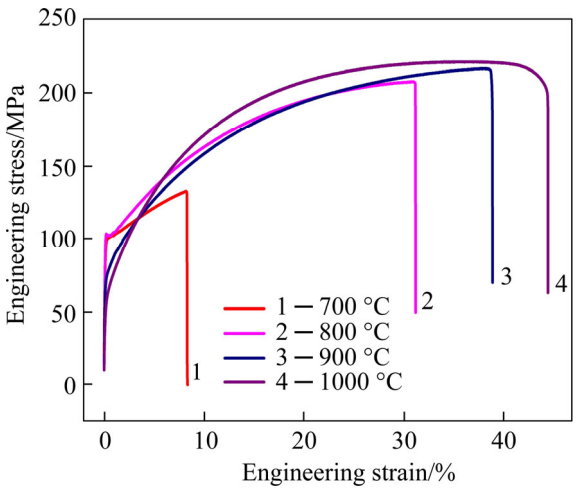

Figure 9 Room temperature engineering strain vs stress curves for sintered samples with atomized copper powder

(EL) increased continuously with the increasing sintering temperature, reaching the maximum at 1000 °C, that is, UTS=223 MPa, YS=70 MPa, EL=60% of electrolytic copper samples, and UTS=221 MPa, YS=64 MPa, EL=44 % of atomized copper samples, respectively. By reference to ASM Handbook, the tensile strength, yield strength and elongation of electrolytic copper sample sintered at 1000 °C are comparable to those the annealed pure copper [42].

The fracture analysis of the tensile specimens was carried out by SEM, and the results are shown in Figures 10 and 11. As can be seen from the fracture morphology of the sample sintered at 700 °C with electrolytic copper powder in Figure 10(a), it shows obviously circular dimple fracture. There are some small irregular particles in the dimples, which was recognized as Cu_2O using EDS analysis. However, this phenomenon did not appear at higher temperature. The sintered neck and pores decrease with the increase of sintering temperature. At the

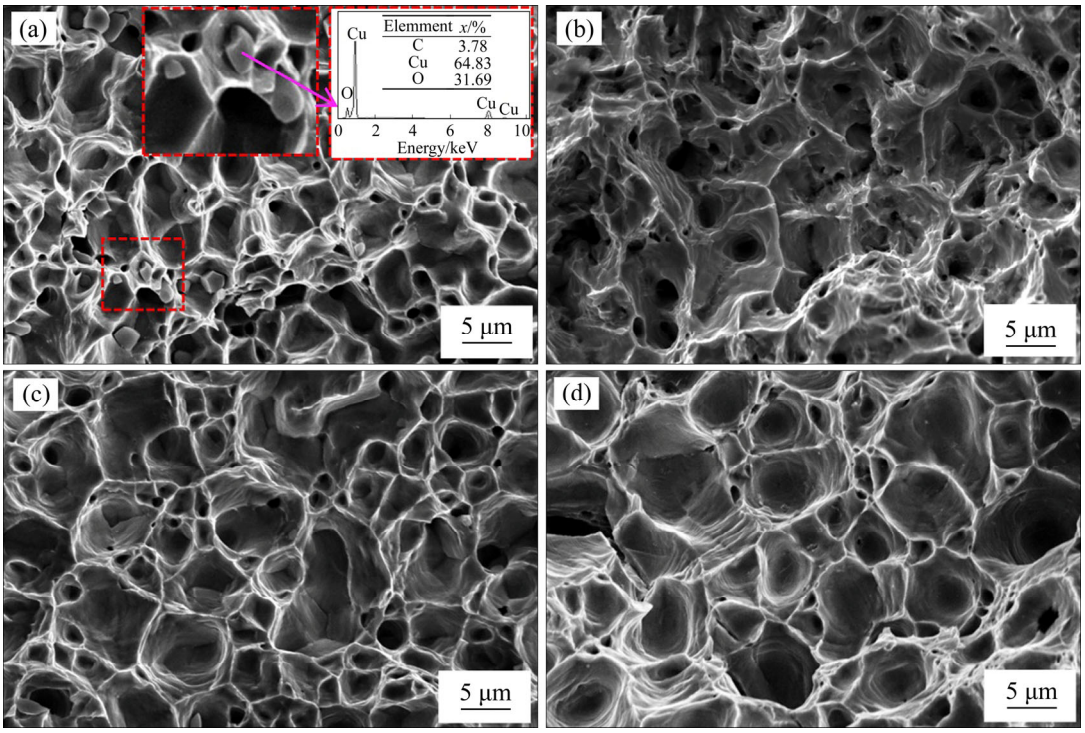

Figure 10 Fracture surfaces of samples sintered at 700 °C (a), 800 °C (b), 900 °C (c) and 1000 °C (d) with electrolytic copper powder

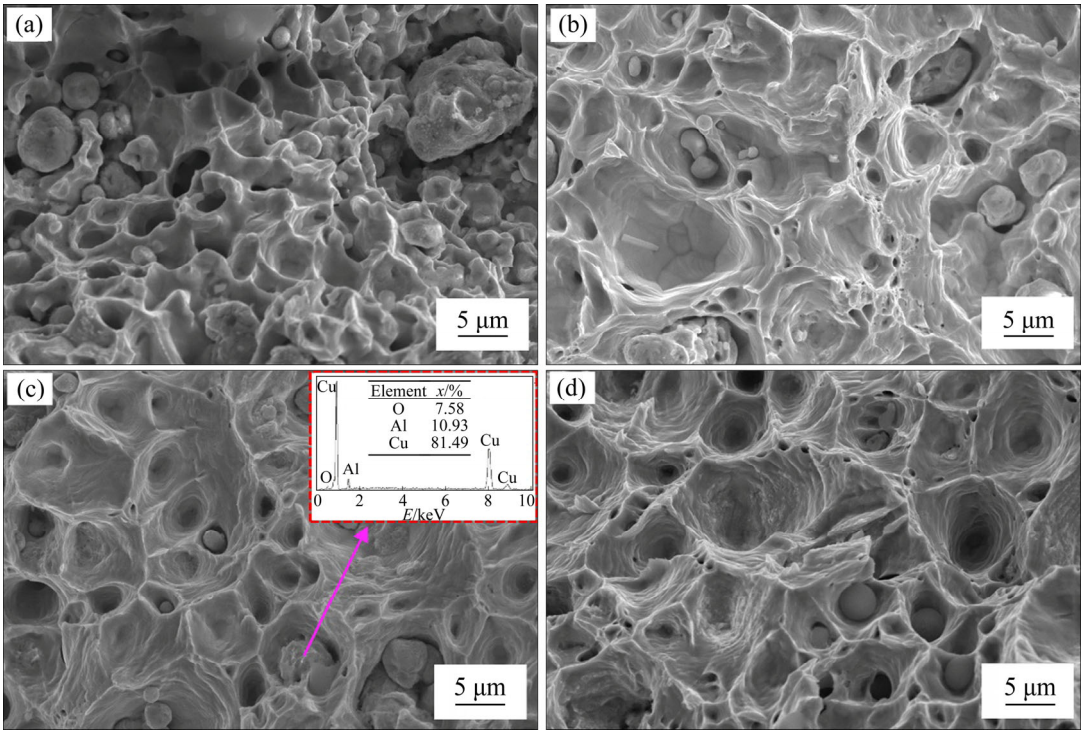

Figure 11 Fracture surfaces of samples sintered at (a) 700 °C, (b) 800 °C, (c) 900 °C and (d) 1000 °C with atomized copper powder

sintering temperature of 1000 °C, most of the fracture area of the sample shows the dimple morphology due to grain tearing, but there are still a few pores. The fracture trend of the sintered sample by atomized copper powder is the same as that of the electrolytic copper powder. The difference is that the sintered necks of atomized copper powder are not as well developed as electrolytic copper, where larger interparticle necks can be seen. However, the atomized copper powder sample has fine powder particles in the dimples shown in Figure 11, and large incomplete sintered powder in Figure 11(b). EDS analysis of the small particles in the dimples shows that there is alumina on the surface of the powder, seen from Figures 11(c) and (d). This indicates that the strength of sintered materials depends on powder bonding. The appearance of fracture for samples sintered at 1000 °C shows the large-area fracture comprising the neck region and the particle body. This led to higher strength than that at the preceding lower sintering temperature due to more load bearing area.

4 Conclusions

The effects of different sintering schedules on the microstructure, density and mechanical properties of samples prepared by electrolytic and water-gas combined atomized copper powder were studied, and the following conclusions are drawn:

1) The sintering capability of the electrolytic copper powder is better than atomized copper powder, which is attributed to the higher sintering driving force from the finer primary particles and the absence of Cu_2O at the grain boundaries.

2) Due to the raw powder with low oxygen content and high residual stress originating from the CIP process, the sintered samples by electrolytic copper powder have smaller grains and preferentially formed twin crystals, compared with the atomized copper powder.

3) Sintered copper samples with electrolytic and water-gas combined atomized copper powder under pressureless hydrogen atmosphere at 1000 °C reach the maximum relative density of 99.3% and 97.4%, respectively. The corresponding mechanical properties are UTS=223 MPa, YS=70 MPa, EL=60% and UTS=221 MPa, YS=64 MPa, EL=44%.

Contributors

LI Pei and CHEN Cun-guang contributed

equally to this work. CHEN Cun-guang and LI Pei conducted the literature review and wrote the draft of the manuscript. QIN Qian, LU Tian-xing and SHAO Yan-ru analyzed the measured data. YANG Fang and HAO Jun-jie edited the draft of manuscript. GUO Zhi-meng provided the concept. All authors replied to reviewers' comments and revised the final version.

Conflict of interest

LI Pei, CHEN Cun-guang, QIN Qian, LU Tian-xing, SHAO Yan-ru, YANG Fang, HAO Jun-jie and GUO Zhi-meng declare that they have no conflict of interest.

References

[1] AGHAMIRI S M S, OONO N, UKAI S, KASADA R, NOTO H, HISHINUMA Y, MUROGA T. Microstructure and mechanical properties of mechanically alloyed ODS copper alloy for fusion material application [J]. Nuclear Materials and Energy, 2018, 15: 17−22. DOI: 10.1016/j.nme.2018.05.019.

[2] ALTENBERGER I, KUHN H A, MÜLLER H R. Material properties of high-strength beryllium-free copper alloys [J]. International Journal of Materials and Product Technology, 2015, 50(2): 124−146. DOI: 10.1504/IJMPT.2015.067820.

[3] PALOMA H M, XIANZHANG L, RUOYU X, MINGYU Z, IAN A K, ROBERT J Y. Copper/graphene composites: A review [J]. Journal of Materials Science, 2019, 54: 12236−12289. DOI: 10.1007/s10853-019-03703-5.

[4] JANKOVIĆ Z. Electrical and thermal properties of poly (methylmetacrylate) composites filled with electrolytic copper powder [J]. International Journal of Electrochemical Science, 2018, 13: 45−57. DOI: 10.20964/2018.01.24.

[5] FILIZ B C. The role of catalyst support on activity of copper oxide nanoparticles for reduction of 4-nitrophenol [J]. Advanced Powder Technology, 2020, 31(9): 3845−3859. DOI: 10.1016/j. apt.2 020.07.026.

[6] YENWISET S, YENWISET T. Effect of the molten metal stream's shape on particle size distribution of water atomized metal powder [J]. Engineering Journal, 2016, 20(1): 187−196. DOI: 10.41 86/ ej.2016.20.1.187.

[7] ALVAREZ K L, MARTÍN J, BURGOS N. Structural and magnetic properties of amorphous and nanocrystalline Fe–Si–B–P–Nb–Cu alloys produced by gas atomization [J]. Journal of Alloys and Compounds, 2019, 810: 151754. DOI: 10.1016/j.jallcom.2019.151754.

[8] HOU Long, LI Ming-rui, JIANG Chao, FAN Xing-du. Thermal and magnetic properties of Fe(Co)BCCu amorphous alloys with high saturation magnetization of 1.77 T [J]. Journal of Alloys and Compounds, 2021, 856: 157071. DOI: 10.1016/j.jallcom.2020.157071.

[9] PAVLOV E A, UDALOVA T A, GRIGOREVA T F. Preparing ultradisperse copper powder via the mechanochemical reduction of copper oxides by magnesium [J]. Bulletin of the Russian Academy of Sciences Physics, 2018, 82(5): 574−577. DOI: 10.3103/S1062873818050234 .

[10] LEDFORD C, ROCK C, CARRIERE P. Characteristics and processing of hydrogen-treated copper powders for EB-PBF additive manufacturing [J]. Applied Sciences, 2019, 9(19): 3993. DOI: 10.3 390/app9193993.

[11] WENDEL J, MANCHILI S K, HRYHA E. Reduction of surface oxide layers on water-atomized iron and steel powder in hydrogen: Effect of alloying elements and initial powder state [J]. Thermochimica Acta, 2020, 692: 178731. DOI: 10.1016/j.tca.2020.178731.

[12] KARLSSON H, NYBORG L, BERG S. Surface chemical analysis of prealloyed water atomised steel powder [J]. Powder Metallurgy, 2005, 48(1): 51−58. DOI: 10.1179/0032589005X37675.

[13] KIM T, OH J M, CHO G H. Surface and internal deoxidation behavior of titanium alloy powder deoxidized by Ca vapor: Comparison of the deoxidation capability of solid solution and intermetallic titanium alloys [J]. Applied Surface Science, 2020, 534: 147623. DOI: 10.1016/j.apsusc.2020.147623.

[14] JUDITHM, YANNICK C, LOÏC P, BENJAMINV, CLAUDE G. Spark plasma sintering and hydrogen pre-annealing of copper nanopowder [J]. Materials Science and Engineering A, 2015, 621: 61−67. DOI: 10.1016/j.msea.2014.10.040.

[15] STENZEL D, SCHWARZER C, SCHNEPF M. Characterization of alternative sinter materials for power electronics [C]// 2019 22nd European Microelectronics and Packaging Conference & Exhibition (EMPC). 2019: 1−8. DOI: 10.23919/EMPC44848.2019.8 951880.

[16] LI Ke-wei, GAO Fei. Heterogeneity of grain refinement and texture formation during pulsed electric current sintering of conductive powder: A case study in copper powder [J]. Advanced Powder Technology, 2018, 29(12): 3385−3393. DOI: 10.1016/j.apt.2018.09.018.

[17] ABE J O, POPOOLA A P I, POPOOLA O M. Consolidation of Ti6Al4V alloy and refractory nitride nanoparticles by spark plasma sintering method: Microstructure, mechanical, corrosion and oxidation characteristics [J]. Materials Science and Engineering A, 2020, 773: 138920. DOI: 10.1016/j.msea.2020.138920.

[18] HIGASHI M, KANNO N. Effect of initial powder particle size on the hot workability of powder metallurgy Ni-based superalloys [J]. Materials & Design, 2020, 194: 108926. DOI: 10.1016/j.matdes.2020.108926.

[19] JIANG R, BULL D, PROPRENTNER D. Effects of oxygen-related damage on dwell-fatigue crack propagation in a P/M Ni-based superalloy: From 2D to 3D assessment [J]. International Journal of Fatigue, 2017, 99: 175−186. DOI: 10.1016/j.ijfatigue.2017.03.003.

[20] SEVOSTYANOV M A, KOLMAKOV A G, SERGIYENKO K V. Mechanical, physical-chemical and biological properties of the new Ti-30Nb-13Ta-5Zr alloy [J]. Journal of Materials Science, 2020, 55(29): 14516−14529. DOI: 10.1007/s10853-020-05020-8.

[21] HIRSCH H H. Improving conductivity of copper PM parts by pretreatment of green compact [J]. Powder Metallurgy, 1979,

22(2): 49−61. DOI: 10.1179/pom.1979.22.2.49.

[22] GUSCHLBAUER R, BURKHARDT A K, FU Z. Effect of the oxygen content of pure copper powder on selective electron beam melting [J]. Materials Science and Engineering A, 2020, 779: 139106. DOI: 10.1016/j.msea.2020.139106.

[23] ZHOU Xiao-long, LI Chen, CAO Han-xing, YU Jie, QIU Guang-huai, WANG Li-hui. Effects of emulsified asphalt on the mechanical and tribological properties of copper/graphite composites [J]. Materials Research Express, 2019, 6(5): 056515. DOI: 10.1088/2053-1591/aafeb7.

[24] MINETA T, SAITO T, YOSHIHARA T. Structure and mechanical properties of nanocrystalline silver prepared by spark plasma sintering [J]. Materials Science and Engineering A, 2019, 754: 258−264. DOI: 10.1016/j.msea.2019.03.101.

[25] CHING N T, HOE C C K, HONG T S, GHOBAKHLOO M. Case study of lean manufacturing application in a die casting manufacturing company [J]. AIP Conference Proceedings, 2015, 1660(1): 090007. DOI: 10.1063/1.4915851.

[26] GIERL C. Reactions between ferrous powder compacts and atmospheres during sintering−An overview [J]. Powder Metallurgy, 2020, 63(4): 237−253. DOI: 10.1080/00325899. 2020.1810427.

[27] ZHANG M X, KELLY P M. The morphology and formation mechanism of pearlite in steels [J]. Materials Characterization, 2009, 60(6): 545−554. DOI: 10.1016/j.matc har.2009.01.001.

[28] BARROS L, POLETTO J, NEIS P. Influence of copper on automotive brake performance [J]. Wear, 2019, 426: 741−749. DOI: 10.1016/j.wear.2019.01.055.

[29] SINGH G, PANDEY P M. Experimental investigations into mechanical and thermal properties of rapid manufactured copper parts [J]. Proceedings of the Institution of Mechanical Engineers, Part C: Journal of Mechanical Engineering Science, 2020, 234(1): 82−95. DOI: 10.1177/0954 406219875483.

[30] ASTM B962-17. Standard test methods for density of compacted or sintered powder metallurgy (PM) products using Archimedes' principle [S]. US, 2017.

[31] SINGH G, PANDEY P M. Topological ordered copper graphene composite foam: fabrication and compression properties study [J]. Materials Letters, 2019, 257: 126712. DOI: 10.1016/j.matlet.2019.126712.

[32] COLLET R, LE G S, CHARLOT F. Oxide reduction effects in SPS processing of Cu atomized powder containing oxide inclusions [J]. Materials Chemistry & Physics, 2016, 173: 498−507. DOI: 10.1016/j.matchemphys.2016.02.044.

[33] WENDEL J, MANCHILI S K, HRYHA E. Sintering behaviour of compacted water-atomised iron powder: Effect of initial state and processing conditions [J]. Powder Metallurgy, 2020, 63(5): 1−11. DOI: 10.1080/00325899. 2020.1833138.

[34] GERMAN R M. History of sintering: Empirical phase [J]. Powder Metallurgy, 2013, 56(2): 117−123. DOI: 10.1179/ 1743290112Y.0000000025.

[35] SCOTT G D. Radial distribution of the random close packing of equal spheres [J]. Nature, 1962, 194: 956−957. DOI: 10.1038/194956a0.

[36] MASON G. Radial distribution functions from small packings of spheres [J]. Nature, 1968, 217: 733−735. DOI: 10.1038/ 217733a0.

[37] ATWATER M A, LUCKENBAUGH T L, HORNBUCKLE B C. Advancing commercial feasibility of intraparticle expansion for solid state metal foams by the surface oxidation and room temperature ball milling of copper [J]. Journal of Alloys and Compounds, 2017, 724: 258−266. DOI: 10.1016/ j.jal lcom.2017.07.029.

[38] COLLET R, GALLET S, CHARLOT F. Oxide reduction effects in SPS processing of Cu atomized powder containing oxide inclusions [J]. Materials Chemistry and Physics, 2016, 173: 498−507. DOI: 10.1016/j.matchemphys.2016.02.044.

[39] NEKOUIE R K, RASHCHI F, JODA N N. Effect of organic additives on synthesis of copper nano powders by pulsing electrolysis [J]. Powder Technology, 2013, 237: 554−561. DOI: 10.1016/j.powtec.2012.12.046.

[40] AVRAMOVIĆ L, MAKSIMOVIĆ V M, BAŠČAREVIĆ Z. Influence of the shape of copper powder particles on the crystal structure and some decisive characteristics of the metal powders [J]. Metals, 2019, 9(1): 56−59. DOI: 10.3390/ met9010056.

[41] NIKOLIĆ N D, ŽIVKOVIĆ P M, PAVLOVIĆ M G. Overpotential controls a morphology of electrolytically produced copper dendritic forms [J]. Journal of the Serbian Chemical Society, 2019, 84(11): 1209−1220. DOI: 10.2298/ JSC190522066N.

[42] SEIFI R, HOSSEINI R. Experimental study of fatigue crack growth in raw and annealed pure copper with considering cyclic plastic effects [J]. Theoretical and Applied Fracture Mechanics, 2018, 94: 1−9. DOI: 10.1016/j.tafmec.2017.12. 003.

(Edited by HE Yun-bin)

中文导读

电解铜粉与雾化铜粉的烧结组织及性能

摘要：本文采用电解法和水气联合雾化法制备出超细铜粉，通过冷等静压、氢气烧结获得全致密铜。细铜粉具有较高的烧结驱动力，促进烧结收缩和致密化。电解铜粉烧结样品的晶粒尺寸小于雾化铜粉，且容易形成孪晶，这是由于电解铜粉氧含量低，冷等静压过程使粉末产生较高残余应力。在 1000 ℃烧结温度下，电解铜粉和雾化铜粉烧结体的相对密度分别达到 99.3%和 97.4%，高于文献报道的粉末冶金铜零件。两种粉末制备的烧结铜的抗拉强度和屈服强度接近，但电解铜粉烧结样品的延伸率(60%)高于水气联合雾化铜粉的烧结样品(44%)。电解铜粉烧结样品的晶界中不含氧化亚铜，因此具有高的密度和低的氧含量，最终获得优异的性能。

关键词：铜粉；电解；水气联合雾化；烧结组织；性能